

# KappaFace: Adaptive Additive Angular Margin Loss for Deep Face Recognition

Chingis Oinar  
Sungkyunkwan University

Binh M. Le  
Sungkyunkwan University

Simon S. Woo  
Sungkyunkwan University

## Abstract

Feature learning is a widely used method employed for large-scale face recognition. Recently, large-margin softmax loss methods have demonstrated significant enhancements on deep face recognition. These methods propose fixed positive margins in order to enforce intra-class compactness and inter-class diversity. However, the majority of the proposed methods do not consider the class imbalance issue, which is a major challenge in practice for developing deep face recognition models. We hypothesize that it significantly affects the generalization ability of the deep face models. Inspired by this observation, we introduce a novel adaptive strategy, called KappaFace, to modulate the relative importance based on class difficulty and imbalance. With the support of the von Mises-Fisher distribution, our proposed KappaFace loss can intensify the margin's magnitude for hard learning or low concentration classes while relaxing it for counter classes. Experiments conducted on popular facial benchmarks demonstrate that our proposed method achieves superior performance to the state-of-the-art.

## 1 INTRODUCTION

Deep Convolutional Neural Networks (DCNN) demonstrated staggering improvements in the field of image representation learning. Hence it has widely been adopted for numerous image related tasks, including face recognition. Recently, it has also been observed that the traditional softmax loss fails to produce highly discriminative feature vectors (Wang et al., 2017). Thus, Deep Metric Learning has received a massive attention and been used for a variety of

tasks, especially face recognition (Schroff et al., 2015; Wen et al., 2016). However, due to high computational costs of the previous methods, such as Triplet Loss, on larger datasets, several variants have been proposed to improve the discriminative power of the softmax loss (Deng et al., 2019; Wang et al., 2018; Liu et al., 2017a; Huang et al., 2020; Wang et al., 2017; Liu et al., 2019a). Therefore, current state-of-the-art methods focus on modulating positive margins to enforce intra-class compactness and inter-class diversity, such as ArcFace (Deng et al., 2019), CosFace (Wang et al., 2018) and SphereFace (Liu et al., 2017a). Furthermore, the fixed margins significantly improved the generalization ability of DCNN, achieving a great performance on a series of major face benchmarks, namely LFW (Huang et al., 2008), CFP-FP (Sengupta et al., 2016), CPLFW (Zheng and Deng, 2018), AgeDB (Moschoglou et al., 2017), CALFW (Zheng et al., 2017), IJB-B (Whitelam et al., 2017) and IJB-C (Maze et al., 2018).

However, recent works, including CurricularFace (Huang et al., 2020), demonstrated previous large margin methods being inefficient for datasets having issues such as class imbalance or sample difficulty within a class. In fact, the class imbalance turns out to be a major challenge faced by deep face recognition models. Thus, the fixed margin methods were shown to produce biased decision boundaries, as demonstrated in (Liu et al., 2019a), owing to which minority classes poorly describe the true feature space.

In this paper, we propose Adaptive Additive Angular Margin Loss (KappaFace) to further tackle these challenges. Unlike some of the recent works, we adopt the von Mises-Fisher distribution (vMF) and present a method based on concentration and population parameters of a training dataset to achieve an adaptable class-based margin loss. The vMF is used for modeling the hyperspherical distribution of instances of a certain class, along with estimation of the class concentration, which reflect its hardness caused by a variation in facial angles, ages, and resolutions. Therefore, we aim to balance additive margins between the classes to improve generalization ability for imbalanced datasets. As shown in Fig. 1, our approach behaves differently across varying scenarios from rugged to easy classes and from scarce to popular classes, demon-

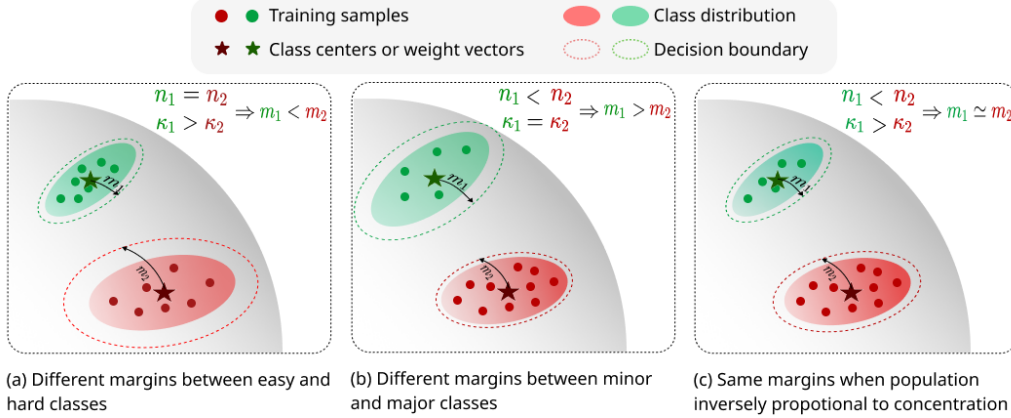


Figure 1: Effects of our adaptive strategy in KappaFace. (a) We prioritize difficult classes by intensifying margins for low concentration classes. (b) Minority classes get relatively larger margins than majority classes do. (c) Finally, we assign a similar importance provided the population of one class is proportional to the concentration of another.

strating our approach is highly adaptive and effective for imbalanced training datasets. Our main contributions are summarized as follows:

- We propose a novel method, KappaFace, which adjusts a class importance by taking both its difficulty and imbalance into account. With the vMF distribution for individual classes, KappaFace relaxes the margin for high concentration classes, while intensifying the margins of hard and underrepresented classes.
- For modeling hyperspherical distributions, we introduce a memory buffer to efficiently update the concentration and population parameters while training as well as modulating the positive margins, without any extra computational costs in the inference stage.
- We evaluate our method on a series of popular face recognition benchmarks and demonstrate that our proposed method consistently outperforms other state-of-the-art counterparts.

## 2 RELATED WORK

**Deep Metric Learning.** Deep Metric Learning (DML) is currently widely adopted for deep face recognition tasks as it was observed to produce highly efficient feature vectors comparing to the traditional softmax loss (Hu et al., 2014; Liu et al., 2017b). Thus, with the increasing attention towards DML, there have been various methods proposed in recent years, albeit some of the eminent works in the area include FaceNet (Schroff et al., 2015), Center Loss (Wen et al., 2016), Circle Loss (Sun et al., 2020), L-Softmax Loss (Liu et al., 2016) and N-pair Loss (Sohn, 2016). However, the methods that require mining of both negative and positive samples, especially Triplet Loss, N-pair Loss and Circle Loss, become extremely computationally costly provided the size of the training set increases considerably.

**Normalization and Spherical Distribution.** Normalization plays a crucial role in current state-of-the-art deep face recognition methods. The majority of works apply  $l_2$  normalization on the weights and the feature vectors to embed them onto a unit hypersphere (Deng et al., 2019; Liu et al., 2017a; Wang et al., 2018; Liu et al., 2019a; Huang et al., 2020). In this fashion, the inner product is replaced by cosine similarity within the softmax loss. Interestingly, it was observed to significantly contribute to the model performance as shown by NormFace (Wang et al., 2017). Furthermore, it was reported that normalization reduces prior caused by the training data imbalance issue (Liu et al., 2017a). Therefore, modeling the hyperspherical distribution of facial features, particularly the von Mises Fisher distribution, has drawn attention from recent works (Hasnat et al., 2017; Zhe et al., 2019; Li et al., 2021). Specifically, they produce the belongingness probability from a predicted or mini-batch estimated concentration. In contrast, we adopt a memory buffer to govern all classes’ concentrations simultaneously. Thereby, we can modulate the concentrations’ diversity and generally adjust our loss upon the relative hardness and imbalance of an individual class.

**Margin-based Loss Function.** Considering that the learned features obtained using the conventional softmax loss were shown not to be discriminative enough for practical face recognition problem, current SOTA deep face recognition methods mostly introduce margin-based loss functions as in (Deng et al., 2019; Liu et al., 2017a; Wang et al., 2018; Liu et al., 2019a; Huang et al., 2020). However, there have been several challenges reported, especially dataset imbalance or sample difficultness, to be common for deep face recognition tasks. Based on this observation, there are several methods that aim to overcome these challenges such as Fair Loss (Liu et al., 2019a) or CurricularFace (Huang et al., 2020) by introducing Reinforcement Learning (RL) agent and negative margin, re-

spectively. However, the introduction of an additional network to train on top of a backbone is not only a non-trivial task, but also a computational overhead to the training procedure. Meanwhile, although the negative margin introduced by CurricularFace addresses the challenge of a sample difficultness, it does not take the class imbalance into account. Thereby, our proposed KappaFace aims to address both challenges, class difficultness and its imbalance, with no additional trainable parameters.

**Class Imbalance.** Class imbalance is a common problem in a deep face recognition. Traditional approaches of tackling the issue include data re-sampling (He and Garcia, 2009) and cost-sensitive learning (Krawczyk et al., 2014; Tang et al., 2008). Furthermore, there are also methods, such as Class-Balanced Loss (Cui et al., 2019), that introduce modifications directly into the classical softmax loss. Although, it might be effective for the classification task in general, it, unfortunately, fails to produce highly discriminative feature vectors, which is vital for such tasks as deep face recognition. However, there have been only a few methods proposed that address the issue. For instance, Liu et al. demonstrate a method, Fair Loss (Liu et al., 2019a), to modulate margins by introducing a RL agent on top of a backbone. On the other hand, our method does not rely on additional networks, which reduces a training cost yet ensures a high generalization ability.

### 3 PROPOSED METHOD

#### 3.1 Preliminary Information on Loss Functions

The traditionally used classification loss function, known as softmax loss, is shown as follows:

$$\mathcal{L}_S = -\log \frac{e^{\mathbf{W}_{y_i}^T \mathbf{z}_i + b_{y_i}}}{\sum_{j=1}^C e^{\mathbf{W}_j^T \mathbf{z}_i + b_j}}, \quad (1)$$

where  $\mathbf{z}_i \in \mathbb{R}^d$  represents the embedding of the  $i$ -th sample corresponding to the  $\mathbf{y}_i$  class,  $\mathbf{y}_i \in \{1, \dots, C\}$ .  $\mathbf{W}_j \in \mathbb{R}^d$  denotes  $j$ -th column of the weight matrix  $\mathbf{W} \in \mathbb{R}^{d \times C}$  and  $\mathbf{b}_j$  is the bias term. In the current practice, however, the bias term  $\mathbf{b}_j$  is set to 0, whereas the weight matrix  $\mathbf{W}$  and the deep feature  $\mathbf{z}_i$  are normalized using  $l_2$  normalisation method as in (Deng et al., 2019; Wang et al., 2018; Liu et al., 2017a). Thus, the modified softmax loss is presented as follows:

$$\mathcal{L}_N = -\log \frac{e^{s(\cos \theta_{y_i})}}{e^{s(\cos \theta_{y_i})} + \sum_{j=1, j \neq y_i}^C e^{s(\cos \theta_j)}}, \quad (2)$$

where  $\theta_j = \angle(\mathbf{W}_j, \mathbf{z}_i)$ ,  $s$  is a scaling factor which is commonly set to 64. Considering that the conventional softmax loss does not result in good discriminative features for practical face recognition task, a wide variety of margin-based methods has been proposed, which can be generalized as

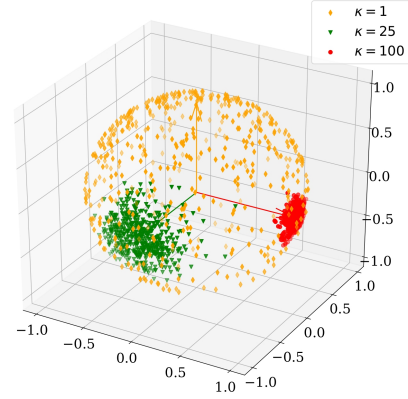


Figure 2: Illustration of von Mises-Fisher (vMF) distribution on 3-dimensional unit sphere.

follows:

$$\mathcal{L}_M = -\log \frac{e^{s(P(\cos \theta_{y_i}))}}{e^{s(P(\cos \theta_{y_i}))} + \sum_{j=1, j \neq y_i}^C e^{s(\cos \theta_j)}}, \quad (3)$$

where  $P(\cos \theta_{y_i})$  is a function to control the positive margin. For instance, ArcFace introduces the function  $P(\cos \theta_{y_i})$  as  $\cos(\theta_{y_i} + m)$ , where  $m$  is an additive angular margin, whereas CosFace and SphereFace introduce additive cosine and multiplicative angular margins, respectively. Thus, utilizing the margin penalties within the softmax loss enforces intra-class compactness and inter-class diversity by penalising a target logit.

However, the proposed methods introduce a fixed margin for all classes without taking the class imbalance into account, which is a common practical challenge for deep face recognition models as discussed in (Liu et al., 2019a). Based on this observation, we introduce a novel approach to dynamically change the relative importance based on a class difficultness as well as its imbalance.

#### 3.2 The von Mises-Fisher distribution

The von Mises-Fisher distribution (vMF) is a probability distribution on the  $d$ -dimensional unit sphere  $\mathbb{S}^{d-1}$ , which has the density function presented as follows (Mardia and Jupp, 2009):

$$p(x|\epsilon, \kappa) = \frac{\kappa^{d/2-1}}{(2\pi)^{d/2} I_{d/2-1}(\kappa)} \exp(\kappa \epsilon^T x), \quad (4)$$

where  $\epsilon \in \mathbb{S}^{d-1}$  is the mean direction,  $\kappa \in \mathbb{R}^+$  is the concentration parameter, and  $I_v$  denotes the modified Bessel function of the first kind at order  $v$  (Temme, 1996). The distribution of samples is uniform on the sphere when  $\kappa = 0$  and more concentrated around the mean direction  $\epsilon$  when  $\kappa$  becomes greater. An illustration of this property is given in Fig.2. Thus, we hypothesize that samples in easy learning classes are scattered around their centers and produce high

concentration values. In contrast, hard learning classes contain noisy or samples having a high variance in terms of facial angles, ages and resolutions resulting in varying concentration values.

To approximate the value of concentration parameter from a set of  $n$  observation samples, [Banerjee et al. \(2005\)](#) propose a simple approximation which follows the maximum likelihood estimation method, and is given by:

$$\hat{\kappa} = \frac{\bar{r}(d - \bar{r}^2)}{1 - \bar{r}^2}, \quad (5)$$

where

$$\bar{r} = \frac{\|\sum_i^n x_i\|_2}{n}. \quad (6)$$

The vMF is used for modeling the sample distributions of the classes in the hyperspherical space. Meanwhile, we can utilize a concentration value  $\hat{\kappa}$  to modulate the angular margin for samples belonging to a certain class.

### 3.3 KappaFace

It is important to emphasize that collecting the feature vectors by the end of each training epoch becomes extremely time-consuming as the size of the training data increases. However, considering that the model is updated every mini-batch, direct use of intermediate feature vectors  $z_i$  will broadly scatter samples, belonging to the same class, on the hypersphere, distorting its true concentration. In order to efficiently estimate the mean direction vectors  $\epsilon$  and concentrations  $\kappa_c$ , we introduce a **memory buffer** that is randomly initialized with the size of  $|\mathcal{D}| \times d$ , where  $|\mathcal{D}|$  denotes the training set's cardinality. Thus, we employ the Exponential Moving Average (EMA) ([Li et al., 2019](#)) to update feature vectors within the memory. Specifically, let  $\bar{z}_i^t$  be the average of the feature vector  $z_i$  for the  $i$ -th sample of the  $t$ -th epoch, hence we update the memory for the epoch  $t+1$  as follows:

$$\bar{z}_i^{t+1} = \alpha \times \bar{z}_i^t + (1 - \alpha) \times z_i, \quad (7)$$

where  $\alpha$  is the momentum parameter. Likewise, the vectors in the memory buffer are normalized following  $l_2$  normalisation. Thus, Eq. 6 can be restated for the  $c$ -th class as follows:

$$\hat{r}_c = \frac{\|\sum_{i|y_i=c} \bar{z}_i\|_2}{n_c}, \quad (8)$$

where the sum of vectors  $\bar{z}_i$  is calculated while training within the memory buffer. This allows us to efficiently compute the concentration values  $\hat{\kappa}_c$  for each class at the end of an epoch using Eq. 5.

Computing individual class margins involves two factors to consider, which are their imbalance and difficultness degrees. Therefore, we present **sample concentration and population weights** that are recalculated once an epoch to

update the final margin values. Initially, the concentration values  $\kappa$  are normalized by subtracting mean and dividing by standard deviation as follows:

$$\mu_\kappa = \frac{\sum_{c=1}^C \hat{\kappa}_c}{C}, \quad (9)$$

$$\sigma_\kappa = \sqrt{\frac{\sum_{c=1}^C (\hat{\kappa}_c - \mu_\kappa)^2}{C}}, \quad (10)$$

$$\tilde{\kappa}_c = \frac{(\hat{\kappa}_c - \mu_\kappa)}{\sigma_\kappa}. \quad (11)$$

Subsequently, the normalized values are used to calculate concentration weights following the formula below:

$$w_c^k = f_k(\tilde{\kappa}_c) = 1 - \sigma(\tilde{\kappa}_c \times T), \quad (12)$$

where  $\sigma$  is a well-known sigmoid function, whereas  $T \in (0, 1)$  is a hyper-parameter that denotes a temperature value.

**Discussion.** The smaller the temperature value, the closer the weights are scattered around 0.5. Also, note that the greater the concentration value than the mean, the smaller the concentration weight  $w_c^k$  and vice versa. Here, the memory buffer plays a crucial role in computing all the concentration values. Thus, we can encourage the concentration values to be closer to the mean and less diverse. Moreover, the class hardness is determined by a relative concentration  $\tilde{\kappa}_c$  over the entire training dataset instead of its true value.

In contrast, considering that the number of samples per class is fixed throughout the training process, there is no need to update the sample weights once they are computed. Thus, the sample weights are obtained as follows:

$$w_c^s = f_s(n_c) = \frac{\cos(\pi \times \frac{n_c}{K}) + 1}{2}, \quad (13)$$

where  $n_c$  is the number of samples for the  $c$ -th class and  $K$  is set to the maximum among them. Illustrations of  $f_k$  and  $f_s$  are given in Fig. 1 in Supp. Section 1.

Finally, the calibration parameter for the margin value of instances belonging to the  $c$ -th class is determined as follows:

$$\psi_c = \gamma w_c^s + (1 - \gamma) w_c^k, \quad (14)$$

where  $\gamma \in (0, 1)$  is a hyper-parameter that balances the scaling contribution of sample concentration and the population. We apply the margin values by utilizing the function proposed by ArcFace. Thus, with  $m_0$  is a fixed initial margin value, the final classification loss looks as follows:

$$\mathcal{L}_K = -\log \frac{e^{s(\cos(\theta_{y_i} + \psi_{y_i} \cdot m_0))}}{e^{s(\cos(\theta_{y_i} + \psi_{y_i} \cdot m_0))} + \sum_{j=1, j \neq y_i}^C e^{s(\cos(\theta_j))}}. \quad (15)$$

Therefore, using 15, we can dynamically adjust the angular margin of a sample upon its class's difficultness and cardinality.

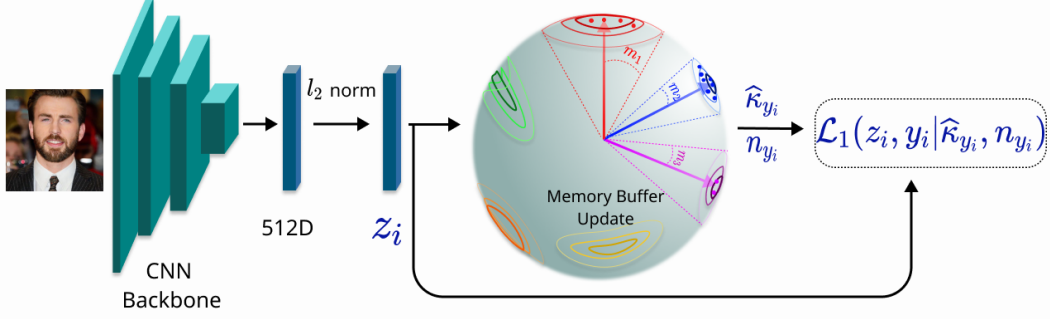


Figure 3: Our overall end-to-end diagram of KappaFace. After forwarding through a CNN backbone, hyper-spherical embedding vector  $z_i$  is fed into our memory buffer for updating  $\kappa_{y_i}$ , and producing scalar  $\psi_{y_i}$ . Our KappaFace loss function can adaptively adjust the margin by including class  $y_i$ 's sample concentration and population, which vary from major to minor classes (e.g.,  $m_2$  and  $m_3$ ) and from hard to easy classes (e.g.,  $m_1$  and  $m_2$ ).

---

**Algorithm 1** KappaFace margin loss training

---

**Require:** Embedding network parameters  $\Theta$ , last fully-connected layer parameters  $\mathbf{W}$ , training dataset  $\mathcal{D}$ , memory buffer  $\mathcal{M}$ , initial margin value  $m_0$ , temperature value  $T$ , learning rate  $\alpha$ .

```

1: while not converged do
2:   for  $x_i, y_i \in \mathcal{D}$  do
3:     # Forward sample and embed to unit sphere
4:      $z_i = \Theta(x_i)$ 
5:      $z_i = z_i / \|z_i\|_2$ 
6:      $\mathbf{W} = \mathbf{W} / \|\mathbf{W}\|_2$ 
7:     # Update  $\mathcal{M}$  by Eq. 7
8:      $\tilde{z}_i \leftarrow \mathcal{M}(z_i, y_i)$ 
9:     # Compute  $\mathcal{L}_K$  by Eq. 15 and update model
10:    loss =  $\mathcal{L}_K(z_i, y_i | \psi_{y_i})$ 
11:     $\Theta \leftarrow \Theta - \alpha \cdot \nabla_{\Theta} loss$ 
12:     $\mathbf{W} \leftarrow \mathbf{W} - \alpha \cdot \nabla_{\mathbf{W}} loss$ 
13:   end for
14:   # Update the scalar  $\psi$  by Eq. 12, 13 and 14
15:    $w^s, w^k \leftarrow \mathcal{M}.update\_weights(T)$ 
16:    $\psi \leftarrow \mathcal{M}.scaling\_factor(w^s, w^k)$ 
17: end while

```

---

### 3.4 Gradient Analysis of KappaFace

In order to provide a comparison with ArcFace, we first define the following theorem about our KappaFace's effectiveness in the training phase, demonstrating it by the gradient analysis below.

**Theorem 1.** *Given  $\{x_i, y_i\}_{y_i=l}$ , then the softmax loss in Eq. 15 provides smaller correction on  $\mathbf{W}$  than ArcFace loss if  $l$  is an easy learning and high concentration class, and greater correction on  $\mathbf{W}$  if  $l$  is a hard learning or low concentration class.*

From Eq. 15, we derive the gradient of our KappaFace loss for one sample  $\{z_i, y_i\}$ ,  $y_i = l \in \{1, \dots, C\}$  with respect to

each  $W_k$  as follow:

$$\begin{aligned} \nabla_{\mathbf{W}_k} \mathcal{L}_K \\ = \begin{cases} -s(1-p_l) \sin(\theta_l + \psi_l m_0) \cdot \nabla_{\mathbf{W}_l} \theta_l, & k = l \\ sp_k \sin \theta_k \cdot \nabla_{\mathbf{W}_k} \theta_k, & k \neq l \end{cases} \end{aligned} \quad (16)$$

where

$$p_j = \frac{\exp(s \cos(\theta_j + \mathbb{1}_l \cdot \psi_l m_0))}{\exp(s \cos(\theta_l + \psi_l m_0)) + \sum_{j=1, j \neq l}^C \exp(s \cos \theta_j)}. \quad (17)$$

For convenience, let  $\mathring{p}_j$  and  $\mathring{m}$  be the probabilities and fixed margin, respectively, corresponding to the ArcFace loss. Then, if  $l$  is an easy learning and high concentration class, the scalar  $\psi_l$  modulates its margin to be smaller than fixed  $\mathring{m}$ . This represents  $p_l > \mathring{p}_l$  and  $p_j < \mathring{p}_j \forall j \neq l$ . If  $k = l$ , then  $\sin(\theta_l + \psi_l m_0) < \sin(\theta_l + \mathring{m}_l)$  provided  $\theta_l$  is small enough,  $\|\nabla_{\mathbf{W}_k} \mathcal{L}_K\|$  of KappaFace loss will be smaller than that of ArcFace loss. If  $k \neq l$ , as  $p_k < \mathring{p}_k \forall k \neq l$ , we achieve the same property of  $\nabla_{\mathbf{W}_k} \mathcal{L}_K$  comparing with the ArcFace loss. In both cases above, we can inversely deduce for the cases of  $l$  being a hard learning or low concentration class.

Finally, our overall method is illustrated in Fig. 3. And we also summarize our end-to-end training process with our proposed KappaFace loss in Algorithm 1. In the validation step, the memory buffer is removed so that the computation expense of our proposed method is similar with the ArcFace.

## 4 EXPERIMENTAL RESULTS

### 4.1 Implementation Details

**Datasets.** We separately utilize CASIA-WebFace (Yi et al., 2014) and refined MS1MV2 (Deng et al., 2019) as our training sets to ensure a fair comparison with other prior state of the art methods. The former dataset, CASIA-WebFace, provides roughly 0.5M images of 10,575 in-

dividuals, whereas the latter one contains approximately 5.8M images of 85,742 identities. We perform computationally extensive experiments on several popular benchmarks, namely LFW (Huang et al., 2008), CFP-FP (Sengupta et al., 2016), CPLFW (Zheng and Deng, 2018), AgeDB (Moschoglou et al., 2017), CALFW (Zheng et al., 2017), YTF (Whitelam et al., 2017), IJB-B (Whitelam et al., 2017), IJB-C (Maze et al., 2018), and MegaFace Challenge 1 (Kemelmacher-Shlizerman et al., 2016).

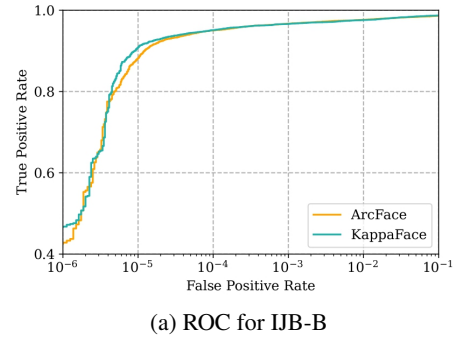
**Training Setting.** For data prepossessing, we follow ArcFace (Deng et al., 2019), and obtain the normalised face crops ( $112 \times 112$ ) by utilizing five landmarks (Zhang et al., 2016; Tai et al., 2019). For the embedding network, we adopt slightly modified versions of the well-known CNN architectures, such as ResNet50 and ResNet100 as evaluated in (Deng et al., 2019). We train models on NVIDIA GeForce RTX 2080 Ti with the batch size of 512. The models are trained using Stochastic Gradient Descent algorithm, with momentum 0.9 and weight decay  $5e - 4$ . On CASIA-WebFace, the learning rate starts with 0.1 and is divided by 10 at 20, 28, and 32 epochs, and the process finishes at 34 epochs. For the larger dataset, we divide the learning rate at 10, 18, and 22 epochs, and finish at 24 epochs. Regarding the memory buffer, we set the momentum  $\alpha = 0.3$ , whereas  $\gamma$  was set to 0.5 and 0.7 for the smaller and the larger dataset, respectively (see Supp. Section 2 for  $\gamma$  setting). All experiments are implemented using PyTorch (Paszke et al., 2019). Additionally, we utilize Partial FC (An et al., 2020), which is a sparse variant of the model parallel architecture for large scale face recognition.

## 4.2 Evaluation Results

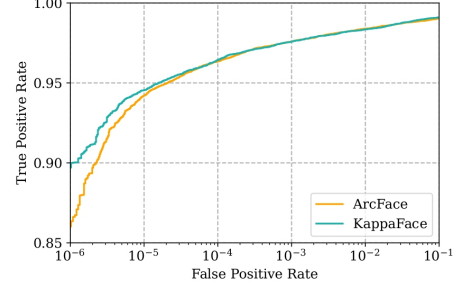
**Results on LFW, CFP-FP, CPLFW, AgeDB, CALFW, and YTF.** We train our KappaFace on MS1MV2 using ResNet100 as a backbone, and provide a comparison with other SOTA methods. In this paper, we follow the unrestricted with labelled outside data protocol, as in (Deng et al., 2019; Huang et al., 2020), to report the results. Additionally, we used 7,000 pair testing images for CFP-FP and 6,000 pairs for the rest of the datasets to report our result similar to (Deng et al., 2019). As reported in Tab. 1, our method attains slightly better results on LFW, YTF and CALFW where the performance is near saturated. However, our KappaFace demonstrates a superiority by outperforming counterparts by an obvious margin on the rest of the datasets, CFP-FP, CPLFW and AgeDB, which could be clearly seen from the table. Similarly, our proposed method achieves a higher accuracy than the ArcFace-SCF (Li et al., 2021), which is the SOTA method that also inherits the spherical distribution properties; however, it is applied on individual samples instead. In particular, we provide an insight on the concentration values we observed throughout the training process in Supp. Section 3.

**Results on IJB-B and IJB-C.** The former dataset, IJB-B, consists of 1,845 identities having 21.8K still images and 55K frames collected from 7,011 videos. There were 10,270 positive pairs and 8M negative pairs used for the 1:1 verification. The latter dataset, IJB-C, is an extension of IJB-B that includes 3,500 subjects with 31K images and 117K frames. There were 19,557 positive pairs, and 15,638, and 932 negative pairs used for the 1:1 verification. Finally, we use our pre-trained KappaFace-MS1MV2-R100 and validate the model on the IJB-B and IJB-C datasets. In Table 2, we provide a comparison in terms of TAR (@ $\text{FAR}=1e^{-4}$ ) with other state-of-the-art methods. Table 2 demonstrates that KappaFace clearly boosts the performance on both datasets by achieving the accuracy of 95.1 and 96.4 on IJB-B and IJB-C, respectively. In Fig. 4, we show the full ROC curves comparing our KappaFace and ArcFace on IJB-B and IJB-C, where our KappaFace demonstrates a staggering improvement in performance over ArcFace even at  $\text{FAR}=1e^{-6}$  establishing a new baseline.

**Results on MegaFace.** Next, we provide an evaluation result on the MegaFace Challenge 1. The gallery set of MegaFace consists of 1M images of 690K unique individuals, and the probe set has 100K photos of 530 subjects from FaceScrub. We report the results under a large training set protocol, where we train ResNet100 on MS1MV2. Note that the results reported are based on the refined MegaFace, where noisy labels are removed. Table 3 clearly shows that



(a) ROC for IJB-B



(b) ROC for IJB-C

Figure 4: ROC of 1:1 verification protocol on IJB-B and IJB-C.

Table 1: Verification performance, in terms of accuracy, results (%) on LFW, YTF, two pose benchmarks (CFP-FP and CPLFW), and two age benchmarks (AgeDB and CALFW).

Method	LFW	CFP-FP	CPLFW	AgeDB	CALFW	YTF
Center Loss (Wen et al., 2016)	99.27	-	81.40	-	90.30	94.9
SphereFace (Liu et al., 2017a)	99.27	-	81.40	-	90.30	95.0
VGGFace2 (Cao et al., 2018)	99.43	-	84.00	-	90.57	-
UV-GAN (Deng et al., 2018)	99.60	94.05	-	-	-	-
ArcFace (Deng et al., 2019)	99.82	98.27	92.08	98.15	95.45	98.0
CurricularFace (Huang et al., 2020)	99.80	98.37	93.13	98.32	96.20	-
ArcFace-SCF (Li et al., 2021)	99.82	98.40	93.16	98.30	96.12	-
KappaFace ( $m = 0.8, T = 0.4$ ) (Ours)	<b>99.83</b>	<b>98.69</b>	<b>93.22</b>	<b>98.47</b>	<b>96.23</b>	<b>98.0</b>

Table 2: 1:1 verification TAR (@ $\text{FAR} = 1e^{-4}$ ) on the IJB-B and IJB-C datasets.

Method	IJB-B	IJB-C
ResNet50+SENet50 (Cao et al., 2018)	80.0	84.1
Multicolumn (Xie and Zisserman, 2018)	83.1	86.2
P2SGrad (Zhang et al., 2019b)	-	92.3
Adacos (Zhang et al., 2019a)	-	92.4
ArcFace-VGG2-R50 (Deng et al., 2019)	89.8	92.1
ArcFace-MS1MV2-R100 (Deng et al., 2019)	94.2	95.6
CurricularFace-MS1MV2-R100 (Huang et al., 2020)	94.8	96.1
KappaFace-MS1MV2-R100 (ours)	<b>95.1</b>	<b>96.4</b>

Table 3: Verification performance, in terms of accuracy, comparison with SOTA methods on MegaFace Challenge 1 using FaceScrub as the probe set. The results reported are based on the refined data. Id corresponds to the rank 1 face identification accuracy with 1M distractors, whereas Ver refers to the face verification TAR at  $1e^{-6}$  FAR.

Method	Id	Ver
AdaptiveFace (Liu et al., 2019b)	95.02	95.61
P2SGrad (Zhang et al., 2019b)	97.25	-
Adacos (Zhang et al., 2019a)	97.41	-
CosFace (Wang et al., 2018)	97.91	97.91
MV-AM-Softmax-a (Wang et al., 2020)	98.00	98.31
ArcFace-MS1MV2-R100 (Deng et al., 2019)	98.35	98.48
CurricularFace-MS1MV2-R100 (Huang et al., 2020)	98.71	98.64
KappaFace-MS1MV2-R100 (ours)	<b>98.77</b>	<b>98.91</b>

the proposed method clearly outperforms other state-of-the-art methods in both identification and verification tasks reaching 98.77 and 98.91, respectively.

### 4.3 Ablation Study

In this section, we use ResNet50 to analyze how our settings for KappaFace on the CASIA-WebFace, which is a highly imbalanced dataset, affect the overall performance and compare it to the ArcFace loss. As we can see in the Table 4, the best setting observed in our series of experiments was  $m_0 = 0.5$ , and  $T = 0.55$ . It is crucial to emphasize that we could not reproduce the exact same results as reported by ArcFace (Deng et al., 2019), hence the results reported are based on our reproduction. However, our proposed KappaFace still shows the robustness and

Table 4: Verification performance, in terms of accuracy, results (%) on popular benchmarks ([CASIA, ResNet50, loss\*])

Loss Functions	LFW	CFP-FP	AgeDB
ArcFace ( $m = 0.5$ )	99.45	95.26	94.45
Ours ( $m_0 = 0.55, T = 0.2$ )	99.43	95.13	<b>94.52</b>
Ours ( $m_0 = 0.5, T = 0.45$ )	99.48	95.26	94.45
Ours ( $m_0 = 0.5, T = 0.55$ )	<b>99.52</b>	<b>95.47</b>	<b>94.52</b>
Ours ( $m_0 = 0.5, T = 0.8$ )	99.35	95.04	94.47
Ours ( $m_0 = 0.5, T = 0.8$ w/o $w^s$ )	99.28	94.97	94.13

improvements over the fixed margin used by the ArcFace loss. Table 4 depicts the verification performance results, measured in terms of accuracy score, on several popular benchmarks, namely LFW, CFP-FP and AgeDB. Table 4 demonstrates that our proposed method outperforms ArcFace in all three evaluation datasets. Interestingly, we observed a slight performance drop after we removed sample weights. Therefore, we can find that both weights, concentration and sample population, contribute to the overall performance as shown in Table 4.

Figure 5 shows the final margin values, obtained by the end of the training procedure, against the number of samples within a class, whereas ArcFace utilizes a fixed margin value of 0.5. Note that minority classes might either be easy, hard or even noisy classes. Hence, there is a wider range of margin values comparing to the majority classes. In fact, CASIA-WebFace dataset contains some

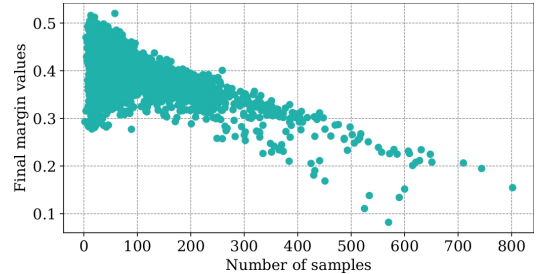
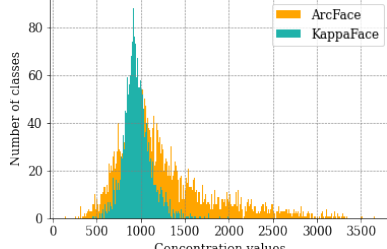
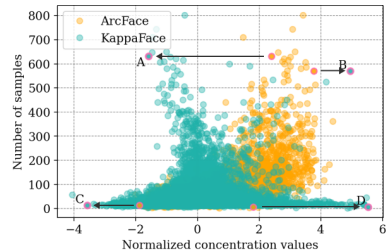


Figure 5: Final additive margin values of KappaFace against number of samples.



(a) Histogram distribution of concentration ( $\hat{\kappa}_c$ ) values against number of classes.



(b) Normalized concentration values ( $\hat{\kappa}_c$ ) against number of samples ( $n_c$ ).

Figure 6: Comparison of final concentration values of ArcFace and KappaFace. A, B, C, and D denote four examples of extreme classes shown in Fig. 7. Arrows indicate changes of relative concentrations from ArcFace to our KappaFace.



(a) Class A:  $\hat{\kappa}_c = -1.58, n_c = 631, \psi_c = 0.42$



(b) Class B:  $\hat{\kappa}_c = 4.96, n_c = 570, \psi_c = 0.15$



(c) Class C:  $\hat{\kappa}_c = -3.56, n_c = 13, \psi_c = 0.93$



(d) Class D:  $\hat{\kappa}_c = 5.44, n_c = 7, \psi_c = 0.52$

Figure 7: Examples from four extreme classes varying from small to high concentration ( $\hat{\kappa}_c$ ), and from underrepresented to overrepresented ( $n_c$ ) ones.

highly noisy classes as it is demonstrated in (Deng et al., 2020).

Next, we provide Fig. 6 that presents the distribution of the final concentration values for both ArcFace and KappaFace. As it can be observed from the sub-figure (a), the mean value of ArcFace is slightly greater; however, the standard deviation also turned out to be larger than that of KappaFace. Moreover, the sub-figure (b) also shows that the normalized concentration values of ArcFace tend to be greater as the number of samples increases. Therefore, this clearly demonstrates that applying the same margin to all classes leads to biased decision boundaries.

From Fig. 6, we select four extreme classes, low concentration - large population (**A**), high concentration - large population (**B**), low concentration - small population (**C**), and low concentration - small population (**D**), and show their samples in Fig. 7 to explain the fundamental causes of the differences. As one may observe, samples from class **A**, collected using a wide range of varying angles, ages and resolutions, produce a concentration of 1.58 standard deviations smaller than the mean yet there are 631 samples available. However, class **B** obtains a high concentration due to a large number of high-quality facial samples. Class **C** contains very noisy samples, hence the concentration value turned out to be low. On the other hand, Class **D** includes only seven high-quality photos having a small variance in terms of facial angles and ages. Therefore, the resulting concentration value is high. From this observation, one may explore further steps on pre-processing the training data to achieve better feature representations; however, it is out of scope of our paper and we leave it for future works.

## 5 CONCLUSION

In this paper, we tackle the problem of deep face recognition in the presence of highly imbalanced challenging dataset and propose a novel Adaptive Additive Margin Loss, KappaFace, which adaptively modulates the positive margins based on class imbalance and difficulty. Our main contribution is decreasing the margin for easy learning and high concentration classes, while increasing the margin for the counter classes by utilizing the von Mises-Fisher (vMF) distribution. Extensive experimental results on popular facial benchmarks reveal that our proposed method consistently outperform other state-of-the-art methods. Moreover, we demonstrate that our adaptive strategy achieves a high generalization ability with highly imbalanced datasets.

## References

An, X., Zhu, X., Xiao, Y., Wu, L., Zhang, M., Gao, Y., Qin, B., Zhang, D., and Ying, F. (2020). Partial fc: Train-

ing 10 million identities on a single machine. In *Arxiv 2010.05222*. 6

Banerjee, A., Dhillon, I. S., Ghosh, J., Sra, S., and Ridge-way, G. (2005). Clustering on the unit hypersphere using von mises-fisher distributions. *Journal of Machine Learning Research*, 6(9). 4

Cao, Q., Shen, L., Xie, W., Parkhi, O. M., and Zisserman, A. (2018). Vggface2: A dataset for recognising faces across pose and age. In *2018 13th IEEE International Conference on Automatic Face Gesture Recognition (FG 2018)*, pages 67–74. 7

Cui, Y., Jia, M., Lin, T.-Y., Song, Y., and Belongie, S. (2019). Class-balanced loss based on effective number of samples. In *Proceedings of the IEEE/CVF conference on computer vision and pattern recognition*, pages 9268–9277. 3

Deng, J., Cheng, S., Xue, N., Zhou, Y., and Zafeiriou, S. (2018). Uv-gan: Adversarial facial uv map completion for pose-invariant face recognition. In *Proceedings of the IEEE conference on computer vision and pattern recognition*, pages 7093–7102. 7

Deng, J., Guo, J., Liu, T., Gong, M., and Zafeiriou, S. (2020). Sub-center arface: Boosting face recognition by large-scale noisy web faces. In *European Conference on Computer Vision*, pages 741–757. Springer. 8

Deng, J., Guo, J., Xue, N., and Zafeiriou, S. (2019). Arcface: Additive angular margin loss for deep face recognition. In *Proceedings of the IEEE/CVF Conference on Computer Vision and Pattern Recognition*, pages 4690–4699. 1, 2, 3, 5, 6, 7

Hasnat, M., Bohné, J., Milgram, J., Gentric, S., Chen, L., et al. (2017). von mises-fisher mixture model-based deep learning: Application to face verification. *arXiv preprint arXiv:1706.04264*. 2

He, H. and Garcia, E. A. (2009). Learning from imbalanced data. *IEEE Transactions on knowledge and data engineering*, 21(9):1263–1284. 3

Hu, J., Lu, J., and Tan, Y.-P. (2014). Discriminative deep metric learning for face verification in the wild. In *Proceedings of the IEEE conference on computer vision and pattern recognition*, pages 1875–1882. 2

Huang, G. B., Mattar, M., Berg, T., and Learned-Miller, E. (2008). Labeled faces in the wild: A database for studying face recognition in unconstrained environments. In *Workshop on faces in 'Real-Life' Images: detection, alignment, and recognition*. 1, 6

Huang, Y., Wang, Y., Tai, Y., Liu, X., Shen, P., Li, S., Li, J., and Huang, F. (2020). Curricularface: adaptive curriculum learning loss for deep face recognition. In *Proceedings of the IEEE/CVF Conference on Computer Vision and Pattern Recognition*, pages 5901–5910. 1, 2, 6, 7

Kemelmacher-Shlizerman, I., Seitz, S. M., Miller, D., and Brossard, E. (2016). The megaface benchmark: 1 million faces for recognition at scale. In *Proceedings of the IEEE conference on computer vision and pattern recognition*, pages 4873–4882. 6

Krawczyk, B., Woźniak, M., and Schaefer, G. (2014). Cost-sensitive decision tree ensembles for effective imbalanced classification. *Applied Soft Computing*, 14:554–562. 3

Li, B., Liu, Y., and Wang, X. (2019). Gradient harmonized single-stage detector. In *Proceedings of the AAAI Conference on Artificial Intelligence*, volume 33, pages 8577–8584. 4

Li, S., Xu, J., Xu, X., Shen, P., Li, S., and Hooi, B. (2021). Spherical confidence learning for face recognition. In *Proceedings of the IEEE/CVF Conference on Computer Vision and Pattern Recognition*, pages 15629–15637. 2, 6, 7

Liu, B., Deng, W., Zhong, Y., Wang, M., Hu, J., Tao, X., and Huang, Y. (2019a). Fair loss: Margin-aware reinforcement learning for deep face recognition. In *Proceedings of the IEEE/CVF International Conference on Computer Vision*, pages 10052–10061. 1, 2, 3

Liu, H., Zhu, X., Lei, Z., and Li, S. Z. (2019b). Adaptiveface: Adaptive margin and sampling for face recognition. In *Proceedings of the IEEE/CVF Conference on Computer Vision and Pattern Recognition*, pages 11947–11956. 7

Liu, W., Wen, Y., Yu, Z., Li, M., Raj, B., and Song, L. (2017a). Sphereface: Deep hypersphere embedding for face recognition. In *Proceedings of the IEEE conference on computer vision and pattern recognition*, pages 212–220. 1, 2, 3, 7

Liu, W., Wen, Y., Yu, Z., and Yang, M. (2016). Large-margin softmax loss for convolutional neural networks. In *ICML*, volume 2, page 7. 2

Liu, X., Vijaya Kumar, B., You, J., and Jia, P. (2017b). Adaptive deep metric learning for identity-aware facial expression recognition. In *Proceedings of the IEEE conference on computer vision and pattern recognition workshops*, pages 20–29. 2

Mardia, K. V. and Jupp, P. E. (2009). *Directional statistics*, volume 494. John Wiley & Sons. 3

Maze, B., Adams, J., Duncan, J. A., Kalka, N., Miller, T., Otto, C., Jain, A. K., Niggel, W. T., Anderson, J., Cheney, J., et al. (2018). Iarpa janus benchmark-c: Face dataset and protocol. In *2018 International Conference on Biometrics (ICB)*, pages 158–165. IEEE. 1, 6

Moschoglou, S., Papaioannou, A., Sagonas, C., Deng, J., Kotsia, I., and Zafeiriou, S. (2017). Agedb: the first manually collected, in-the-wild age database. In *Proceedings of the IEEE Conference on Computer Vision and Pattern Recognition Workshops*, pages 51–59. 1, 6

Paszke, A., Gross, S., Massa, F., Lerer, A., Bradbury, J., Chanan, G., Killeen, T., Lin, Z., Gimelshein, N., Antiga, L., et al. (2019). Pytorch: An imperative style, high-performance deep learning library. *Advances in neural information processing systems*, 32:8026–8037. [6](#)

Schroff, F., Kalenichenko, D., and Philbin, J. (2015). Facenet: A unified embedding for face recognition and clustering. In *Proceedings of the IEEE conference on computer vision and pattern recognition*, pages 815–823. [1, 2](#)

Sengupta, S., Chen, J.-C., Castillo, C., Patel, V. M., Chellappa, R., and Jacobs, D. W. (2016). Frontal to profile face verification in the wild. In *2016 IEEE Winter Conference on Applications of Computer Vision (WACV)*, pages 1–9. IEEE. [1, 6](#)

Sohn, K. (2016). Improved deep metric learning with multi-class n-pair loss objective. In *Advances in neural information processing systems*, pages 1857–1865. [2](#)

Sun, Y., Cheng, C., Zhang, Y., Zhang, C., Zheng, L., Wang, Z., and Wei, Y. (2020). Circle loss: A unified perspective of pair similarity optimization. In *Proceedings of the IEEE/CVF Conference on Computer Vision and Pattern Recognition*, pages 6398–6407. [2](#)

Tai, Y., Liang, Y., Liu, X., Duan, L., Li, J., Wang, C., Huang, F., and Chen, Y. (2019). Towards highly accurate and stable face alignment for high-resolution videos. In *Proceedings of the AAAI Conference on Artificial Intelligence*, volume 33, pages 8893–8900. [6](#)

Tang, Y., Zhang, Y.-Q., Chawla, N. V., and Krasser, S. (2008). Svms modeling for highly imbalanced classification. *IEEE Transactions on Systems, Man, and Cybernetics, Part B (Cybernetics)*, 39(1):281–288. [3](#)

Temme, N. M. (1996). *Special functions: An introduction to the classical functions of mathematical physics*. John Wiley & Sons. [3](#)

Wang, F., Xiang, X., Cheng, J., and Yuille, A. L. (2017). Normface: L2 hypersphere embedding for face verification. In *Proceedings of the 25th ACM international conference on Multimedia*, pages 1041–1049. [1, 2](#)

Wang, H., Wang, Y., Zhou, Z., Ji, X., Gong, D., Zhou, J., Li, Z., and Liu, W. (2018). Cosface: Large margin cosine loss for deep face recognition. In *Proceedings of the IEEE conference on computer vision and pattern recognition*, pages 5265–5274. [1, 2, 3, 7](#)

Wang, X., Zhang, S., Wang, S., Fu, T., Shi, H., and Mei, T. (2020). Mis-classified vector guided softmax loss for face recognition. In *Proceedings of the AAAI Conference on Artificial Intelligence*, volume 34, pages 12241–12248. [7](#)

Wen, Y., Zhang, K., Li, Z., and Qiao, Y. (2016). A discriminative feature learning approach for deep face recognition. In *European conference on computer vision*, pages 499–515. Springer. [1, 2, 7](#)

Whitelam, C., Taborsky, E., Blanton, A., Maze, B., Adams, J., Miller, T., Kalka, N., Jain, A. K., Duncan, J. A., Allen, K., et al. (2017). Iarpa janus benchmark-b face dataset. In *proceedings of the IEEE conference on computer vision and pattern recognition workshops*, pages 90–98. [1, 6](#)

Xie, W. and Zisserman, A. (2018). Multicolumn networks for face recognition. *arXiv preprint arXiv:1807.09192*. [7](#)

Yi, D., Lei, Z., Liao, S., and Li, S. Z. (2014). Learning face representation from scratch. *arXiv preprint arXiv:1411.7923*. [5](#)

Zhang, K., Zhang, Z., Li, Z., and Qiao, Y. (2016). Joint face detection and alignment using multitask cascaded convolutional networks. *IEEE Signal Processing Letters*, 23(10):1499–1503. [6](#)

Zhang, X., Zhao, R., Qiao, Y., Wang, X., and Li, H. (2019a). Adacos: Adaptively scaling cosine logits for effectively learning deep face representations. In *Proceedings of the IEEE/CVF Conference on Computer Vision and Pattern Recognition*, pages 10823–10832. [7](#)

Zhang, X., Zhao, R., Yan, J., Gao, M., Qiao, Y., Wang, X., and Li, H. (2019b). P2sgrad: Refined gradients for optimizing deep face models. In *Proceedings of the IEEE/CVF Conference on Computer Vision and Pattern Recognition*, pages 9906–9914. [7](#)

Zhe, X., Chen, S., and Yan, H. (2019). Directional statistics-based deep metric learning for image classification and retrieval. *Pattern Recognition*, 93:113–123. [2](#)

Zheng, T. and Deng, W. (2018). Cross-pose lfw: A database for studying cross-pose face recognition in unconstrained environments. *Beijing University of Posts and Telecommunications, Tech. Rep*, 5:7. [1, 6](#)

Zheng, T., Deng, W., and Hu, J. (2017). Cross-age lfw: A database for studying cross-age face recognition in unconstrained environments. *arXiv preprint arXiv:1708.08197*. [1, 6](#)